Wake of a Compressor Cascade with Tip Gap, Part 3: Two-Point Statistics

Christian W. Wenger,* William J. Devenport,† Kenneth S. Wittmer,‡ and Chittiappa Muthanna§
Virginia Polytechnic Institute and State University, Blacksburg, Virginia 24061

Velocity spectra and space–time correlations have been measured downstream of a low-speed linear compressor cascade with tip gap. The objective of this work is an improved understanding of the coherent turbulence structures present in fan wakes and of the turbulent source terms responsible for broadband stator noise. The two-point measurements show no correlation between turbulent motions in the wakes or leakage vortices shed by adjacent blades and that the leakage vortex is not subject to low-frequency wandering motions. They also show that the tip leakage vortex turbulence is highly anisotropic and characterized by elongated eddies inclined at about 30 deg to the vortex axis. The presence of such structures, which produce no clearly identifiable footprint in velocity spectra, appears consistent with the helical structures seen in direct numerical simulations of a line vortex with unstably large streamwise velocity defect. This suggests the same mechanism is behind the generation of turbulence in this vortex. Examination of the correlation data from the point of view of a hypothetical stator blade suggests that, because of the anisotropy in turbulence structure, velocity correlations seen by a stator in a real engine are likely to be a strong function of engine geometry and operating point.

Introduction

THIS paper is our third in a series dealing with the flow downstream of a linear compressor cascade. This cascade is designed to reproduce, in an idealized setting, some of the important conditions experienced in the subsonic fan of a large-bypass-ratio aircraft engine, specifically the mechanisms leading to the generation and evolution of the tip leakage vortices that dominate the casing endwall flow, which impinges on the bypass stator. Our first two papers[1,2] focused on single-point velocity measurements of the mean flow and Reynolds-stress fields produced by the blade wakes, the leakage vortices, and the associated endwall flow, as functions of streamwise position, tip gap, and relative motion between the blade tips and endwall. Such measurements provide data and understanding to aid in the development and testing of computational-fluid-dynamics (CFD) prediction tools for calculation of the unsteady aerodynamics and tone noise produced by the stator interaction. In this paper we focus on two-point turbulence measurements. This type of information not only provides insight into the scale and form of the coherent structures that populate the turbulent regions, but is also critical to understanding the generation of broadband noise by the stator row.

To predict the broadband rotor/stator interaction noise, it is, in principle, necessary to have a complete description of the rotor wake turbulence in terms of its two-point space–time correlation function and a response model for the blade row. Complete two-point information is rarely available even for relatively simple flows and cannot be provided by performing Reynolds-averaged CFD calculations. Drastic assumptions about the form of the two-point cor-

relation function are therefore made. Specifically, correlation functions based on the von Kármán spectrum for isotropic homogeneous turbulence are usually assumed,[3,4] even though neither of these adjectives fits the fan wake flow.

The objective of the present paper is an improved understanding of the two-point space–time correlation function of fan-tip wakes and thus of the coherent turbulence structures present in them. Our approach is to use the Virginia Tech Compressor Cascade as an idealized model of the engine flow. Through single- and two-point measurements in this flow, we have been able to observe the form and source of the turbulence and provide a benchmark database for the calibration and testing of prediction methods. We have also been able to examine the turbulence from the point of view of its potential to produce broadband noise and highlight some of the difficulties that predicting that noise might involve.

Background to the Two-Point Measurements

Measurements were made in the same eight-blade linear cascade facility described in Part 1 (Ref. 1), using the same hot-wire instrumentation and procedures. Two-point measurements were made by simultaneously using two of the three-component hot-wire systems described in Part 1. The cascade blades (Fig. 1), chosen because they produce a loading similar to that seen in an aircraft engine fan, produce 12.5 deg of turning. The blades are mounted through the upper wall of the tunnel with their tips resting a short distance above the plane endwall. Blade spacing, chord, and axial chord c_a are, respectively, 236, 254, and 139 mm. Blade span is 254 mm, less the tip gap of 4.0 mm (1.6% chord). Endwall boundary-layer thickness measured midpassage at the cascade inlet is 5.6 mm. The inlet velocity U_∞ was 25.8 ± 0.04 m/s, giving a chord Reynolds number of $3.90 \times 10^5 \pm 2.5 \times 10^3$. A blade-row-aligned coordinate system (X, y, Z) is used to define positions, and an outflow aligned system (x, y, z) is used to define the mean and fluctuating velocity components (U, V, W) and (u, v, w) (see Fig. 1). The origin of the (X, y, Z) system is at the endwall, midway between the leading edges of blades 4 and 5 that frame the center cascade passage.

Measurements were made without relative motion between the blade tips and endwall, that is, without use of the belt system described in Part 2 (Ref. 2). Simultaneously maintaining eight hot-wire sensors and a high-speed belt was simply not practical. The relevance of measurements made without endwall motion was established in Part 2 (Ref. 2). Here it was found that, regardless of wall motion, the development of the tip leakage vortices that dominate the endwall region is controlled by the streamwise mean velocity

*Graduate Assistant, Department of Aerospace and Ocean Engineering, 215 Randolph Hall.
†Professor, Department of Aerospace and Ocean Engineering, 215 Randolph Hall. Senior Member AIAA.
‡Engineer, Department of Aerospace and Ocean Engineering; currently Manager, Aero/Thermo Handling Qualities and Flight Controls, Sikorsky Aircraft, Stratford, CT 06497. Member AIAA.
§Graduate Assistant, Department of Aerospace and Ocean Engineering, 215 Randolph Hall. Student Member AIAA.
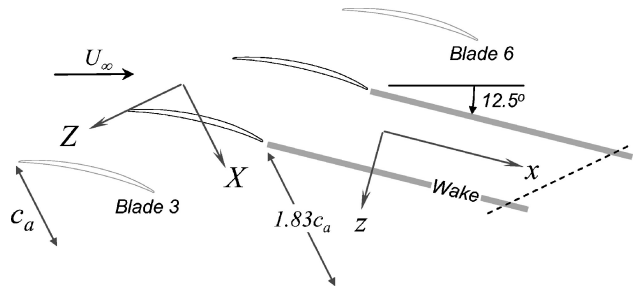
Fig. 1 Schematic of the cascade central passages and definition of coordinate systems (*y* coordinate is measured out of paper from the endwall beneath the blade tips): - - - -, plane of two-point turbulence measurements.

deficit inside them and the turbulence it produces. Wall motion has little effect on the magnitude of this deficit, its decay with downstream distance, and the peak turbulence levels it generates in the vortex. Thus, although endwall motion distorts and displaces the tip leakage vortices it does not alter the fundamental mechanisms controlling their turbulent development. It is the coherent structure associated with these mechanisms that is the primarily focus of the two-point measurements presented here.

The flow conditions just given correspond to those of the baseline flow described in detail in Part 1. In that paper single-point measurements of mean velocity, Reynolds stresses, and triple products made in four cross sections downstream of the central passage of the cascade (at $X/c_a = 1.37, 2.06, 2.83, 3.77$) were described. Here c_a is the axial blade chord of 139 mm. Relevant results, along with some velocity spectra, are summarized here to provide context for the two-point data.

Figures 2a and 2b show contours of mean velocity U/U_∞ and of turbulence kinetic energy k/U_∞^2 (half the sum of the turbulence normal stresses) measured at $X/c_a = 2.83$. The contours clearly show the vertical wakes of blades 4 and 5, located near $Z/c_a = -3.1$ and -4.8, and the region occupied by the tip leakage vortex shed by blade 4. Away from the endwall the wakes are almost two dimensional and grow in a roughly self-similar fashion with distance downstream.[1] They also display the near-Gaussian streamwise mean velocity profile, double-peaked $\bar{u}^2$ and antisymmetric $\overline{uw}$ profiles that are characteristic of fully developed wakes. Close to the endwall, the flow is dominated by the leakage vortex, centered near $y/c_a = 0.12$, $Z/c_a = -4.35$. Consistent with the relatively light loading on the blades, the tip leakage vortex generates a weak swirling flowfield, but a strong streamwise mean velocity deficit (Fig. 2a). Peak tangential velocities produced by the vortex are only about $4.5\% U_\infty$, whereas the peak axial velocity deficit at its center is about 22% U_∞. In a free vortex such a large ratio of axial velocity deficit to peak tangential velocity would render the vortex unstable to helical disturbances.[5] This instability generates helical turbulent structures and mixing that acts to diffuse the axial velocity deficit.[6]

The tip leakage vortex is indeed a center of turbulent activity as evidenced by the turbulence kinetic energy contours of Fig. 2b. Turbulence levels in the vortex are considerably greater than those in the blade wakes and decay at a slower rate with distance downstream (see Part 1, Fig. 13c) making this the dominant source of turbulence further downstream. Contours of turbulence production reveal that most turbulence is being generated in an arc-shaped region above and to the right of the core region. Almost all of this turbulence production is associated with gradients of mean streamwise velocity, and very little is produced by the swirling motions—a result consistent with the mean velocity measurements and the free vortex analogy.

Figure 3 shows sample normalized autospectra of velocity fluctuations measured at the locations shown in Fig. 2a, in the wake of blade 4 and the tip leakage vortex. The spectra are plotted against the nondimensional angular frequency $\omega c_a/U_e$ and normalized so that they integrate to the mean square velocity fluctuations $\bar{u}^2/U_\infty^2$, $\bar{v}^2/U_\infty^2$, and $\bar{w}^2/U_\infty^2$. Here U_e is the velocity of the potential core downstream of the cascade, equal to $0.74U_\infty$. For the most part the spectra have the broadband character typical of fully turbulent
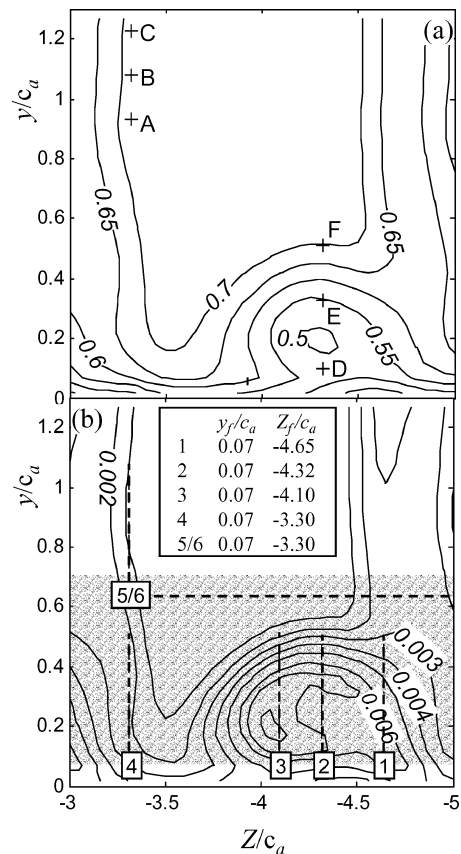
Fig. 2 Flow properties at $X/c_a = 2.83$: a) mean streamwise velocity U/U_∞ and b) turbulence kinetic energy k/U_∞^2. Letters in panel *a* show locations of autospectra plotted in Fig. 3. Dashed lines in panel *b* show profiles along which two-point measurements were made from the anchor locations marked by the numbered squares. Gray region in panel *b* shows extent of two-point measurement grid associated with anchor location 2.
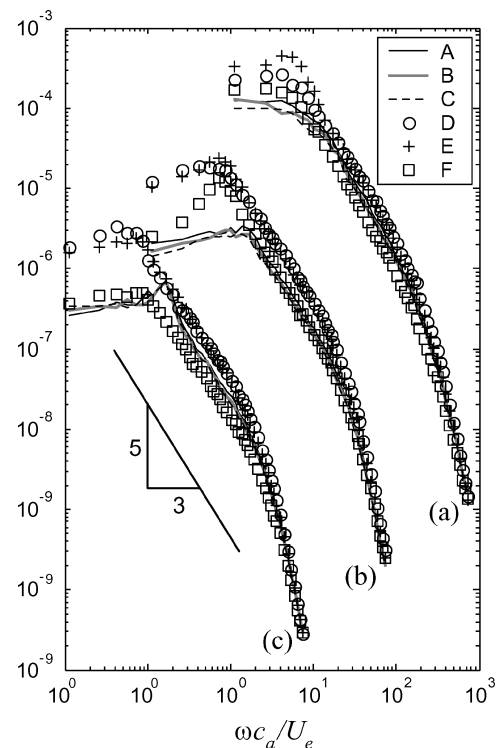
Fig. 3 Autospectra of velocity fluctuations at the six locations identified in Fig. 2a: a) $G_{uu}U_e/U_\infty^2 c_a$, b) $G_{vv}U_e/U_\infty^2 c_a$, and c) $G_{ww}U_e/U_\infty^2 c_a$. Spectral density G defined in Eq. (1) for $\Delta y = \Delta Z = 0$.

flows and display the $-5/3$ slope of the inertial subrange. Spectra measured in the wake of blade 4 (points A, B, and C) appear much like those measured in a plane two-dimensional wake.[7] The spectra measured in the tip leakage vortex (D, E, and F) are remarkable for their lack of features. Spectral levels here are higher than in the wake because of the higher turbulence levels, but there are no distinct spectral peaks that might indicate a periodically organized structure. The spectra also do not show the extreme concentration of energy at very low frequencies as would be expected if the vortex were wandering significantly.[8] In fact, the two-point measurements presented next provide conclusive evidence that wandering was not present.

Two-Point Results

Two-point measurements were made in this baseline flow at $X/c_a = 2.83$ to reveal the scales and orientation of eddies contributing to the endwall turbulence and to examine the implications of this structure for the generation of broadband stator noise in aircraft engines. The measurements were made using two four sensor hot-wire probes, holding one of the probes fixed, while the other probe was traversed over a profile or grid of points (Fig. 2b). For each point, 150 records of 3072 velocity samples were measured at a sampling rate of 50 kHz over a total sampling time of about two minutes. Uncertainties in measurements are presented in Table 1.[9]

The measurements were first processed by taking the fast Fourier transform of the velocity time series and using them to compute the nine-component cross-spectrum tensor between the fixed and traversing probes as a function of the probe separation Δy and ΔZ, for example,

$$G_{uu}(y, \Delta y, Z, \Delta Z, \omega)$$

$$= \lim_{\tau \to \infty} (\pi/T) E[u^*(y, Z, \omega)u(y + \Delta y, Z + \Delta z, \omega)] \qquad (1)$$

with similar expressions for $G_{vv}, G_{ww}, G_{uv}, G_{vw},$ and G_{uw}. A second Fourier transform can then be taken with respect to distance (either Δy, ΔZ or a combination) to yield a wave-number frequency spectrum, for example,

$$\phi_{uu}(y, k_y, Z, \Delta Z, K_x)$$

$$= \frac{U_e}{2\pi} \int_{-\infty}^{\infty} G_{uu}(y, \Delta y, Z, \Delta Z, \omega)e^{-jk_y\Delta y}\, d\Delta y \qquad (2)$$

where $K_x = \omega/U_e$. Such spectra can provide data for a broadband noise calculation but do not provide much intuitive feel for the turbulence structure. A more physical presentation of the data is obtained by taking the inverse Fourier transform of G_{uu} to obtain the (circular) space–time correlation coefficient function

$$R_{uu}(y, \Delta y, Z, \Delta Z, \tau)$$

$$= \int_{-\infty}^{\infty} G_{uu}(y, \Delta y, Z, \Delta Z, \omega)e^{j\omega t}\, d\omega \Big/ \overline{u^2(y, Z)} \qquad (3)$$

Two-Point Profiles

The locations of the two-point profiles are marked in Fig. 2b. For each profile the fixed probe location (y_f, Z_f) is shown by the numbered square, and the associated dashed line is drawn through the corresponding traversing probe positions. Profiles 1–4 are spanwise profiles that were measured to reveal the structure of the turbulence in the endwall region and its pitchwise Z uniformity, particularly in and around the leakage vortex. Profile 5 was measured to examine the spanwise correlation length scales in the straight part of

the blade wake. Profile 6, a pitchwise profile with the same anchor point as profile 5, was chosen to investigate the extent to which the wakes of adjacent blades were correlated. None of the profile 6 measurements showed significant correlation at any time delay. We therefore conclude that the blade wakes were not subject to any correlated unsteadiness. All spanwise profiles (1–5) consisted of 20 to 30 two-point measurements. A minimum probe separation of 3.8 mm $(0.027c_a)$ was used with an increment of 1.3 mm $(0.009c_a)$ for small probe separations. For larger separations, step size was increased to a maximum of 10 mm $(0.073c_a)$. Figure 2 includes a table of anchor-point locations.

The spanwise space–time cross-correlation coefficient results $R(y_f, \Delta y, Z_f, 0, \tau)$ are plotted in Fig. 4 against $\Delta y/c_a$ and $\tau U_e/c_a$.
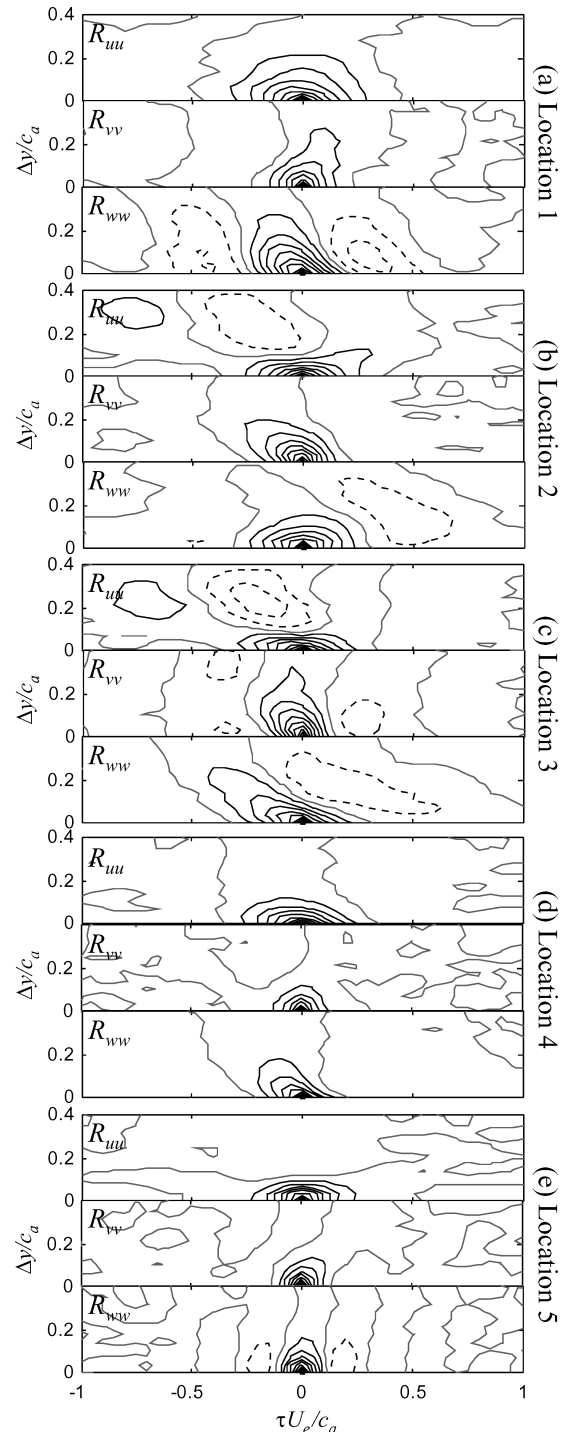

Fig. 4 Comparison of spanwise space–time correlation coefficient functions for the five anchor locations in Fig. 2b. Contours in steps of 0.1: dashed lines, negative levels; black, positive levels; and gray, zero.

Table 1   Uncertainty estimates at 20:1 odds estimated using the method of Kline and McClintock[9]

Quantity	Uncertainty
U	$0.01U_\infty$
k	$0.0005U_\infty^2$
R_{uu}, R_{vv}, R_{ww}	0.03
G_{uu}, G_{vv}, G_{ww}	7%

If one were to apply Taylor's hypothesis to these correlations, τU_e would represent distance in the mean-flow direction. The extent of the correlation functions for profiles 1–3 suggest the presence of significant large-scale structure within the tip leakage vortex flow. This structure is highly anisotropic both in terms of the dissimilarity between the correlations of different velocity components and in terms of the scales of the various correlation functions, which in most cases are a strong function of direction. Specifically, they show u and w velocity fluctuations over the lower half of the vortex $(\Delta y/c_a < 0.13)$ to be well correlated with those at the fixed-probe locations for significant time delays. (Note that, with the present sign conventions, a positive time delay indicates an event occurring at the moving probe location before it is seen at the fixed probe.) The w component correlations in particular show evidence of negative side lobes centered at nondimensional time delays of about $0.4c_a$. These are most clear in profile 1. The v-velocity fluctuations correlate for significantly shorter times, but over a slightly greater range of probe separations.

Profiles 4 and 5, measured in the blade wake, show smaller correlation lengths, especially in v and w. The semicircular contours in profile 5 suggest that the turbulence in the upper part of the blade wake is fairly isotropic. The R_{ww} component at location 5 shows alternate positive and negative lobes along the time axis that suggest some quasi-periodicity in the large scale.

Two-Point Grid

Roughly 600 two-point measurements were taken in a grid over the region indicated by the shaded area in Fig. 2b. For this
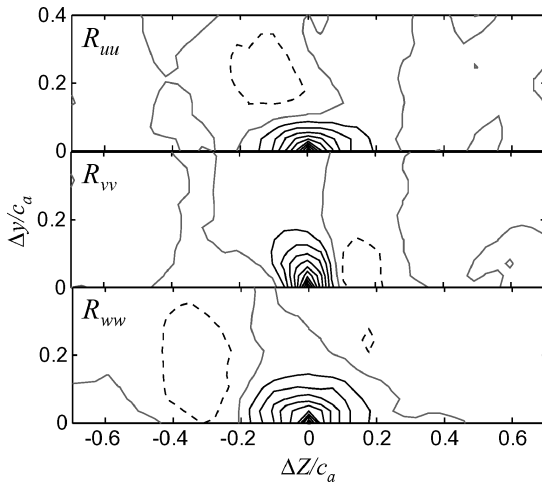

Fig. 5   Spanwise-pitchwise $(\Delta y - \Delta Z)$ correlation coefficient functions for anchor location 2 (see Fig. 2b). Contours in steps of 0.1: black, positive levels and gray, zero.

data set, the fixed probe was positioned at location 2 ($Z_f/c_a = -4.32$, $y_f/c_a = 0.07$) just below the vortex center at $Z/c_a = -4.35$, $y_f/c_a = 0.12$. A minimum probe separation of 3.8 mm ($0.027c_a$) with an increment of 1.3 mm ($0.009c_a$) was used for small probe separations. For larger separations, step size was increased to a maximum of 10 mm ($0.073c_a$).

Calculating the cross correlation for every two-point measurement in the grid results in a three-dimensional correlation space. The axes of the correlation space are the Δy and ΔZ coordinates, which give the movable probe location relative to the fixed probe, and the time-delay coordinate τ. This space can be examined by looking at two-dimensional slices. One such slice, already presented in Fig. 4b, is the spanwise time-delay correlation function $R(0.07c_a, \Delta y, -4.32c_a, 0, \tau)$. A second slice, the zero-time-delay correlation function $R(0.07c_a, \Delta y, -4.32c_a, \Delta Z, 0)$, is presented in Fig. 5. Consistent with the spanwise correlation, this picture shows u and w velocity fluctuations over the lower half of the vortex ($\Delta y < 0.13$) to be well correlated with those at the fixed-probe locations for Z separations up to about $0.2c_a$, one-quarter of the width of the turbulent region generated by the vortex. These correlations indicate the coherence of the turbulent fluctuations in the flow swept across the wall by the tip leakage vortex. The v correlations are more localized in Z but extend farther from the wall, to just above the vortex center location. None of the correlation measurements made at large probe separation ($|\Delta Z/c_a > 0.7|$) showed any significant values. In particular, we detected no correlation at any time delay between velocity fluctuations in the adjacent tip leakage vortices shed from blades 4 and 5.

The full, three-dimensional character of the space–time correlation function becomes more apparent when we examine the third orthogonal slice, the Z-wise time-delay correlation function $R(0.07c_a, 0, -4.32c_a, \Delta Z, \tau)$, shown in Fig. 6. The correlations in this plane extend much farther than in the other two and for all components are concentrated in an elliptical region whose major axis extends diagonally across the plane. In all components the correlation function is highly anisotropic, the major axis of the ellipse extending five to six times farther than its minor axis. Interestingly, the pitchwise extent of this correlation, from about $\Delta Z/c_a = -0.5$ to 0.5, is roughly equal to the pitchwise extent of the vortex itself (Fig. 2b). This suggests the presence of coherent structures or other organized motions involving the whole vortex. The timewise extent of the correlation, from about $\tau U_e/c_a = -0.5$ to 0.7, implies (given Taylor's hypothesis) that these motions have a similar scale in the streamwise direction. The coherent motions responsible for these correlations therefore cannot be wandering, as that would imply side-to-side motions of the vortex on a streamwise scale much longer than its width.

To explain these remarkable correlation maps, it is necessary to visualize the full three-dimensional form of the correlation function. An effective way of doing this is to use the correlation function
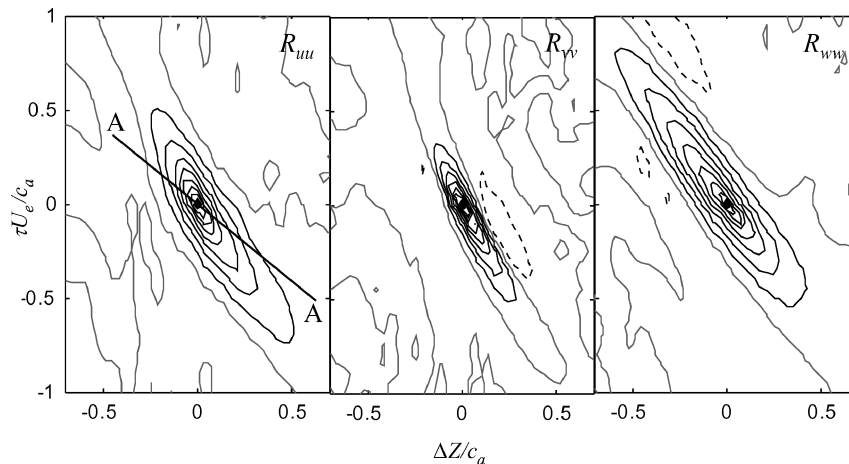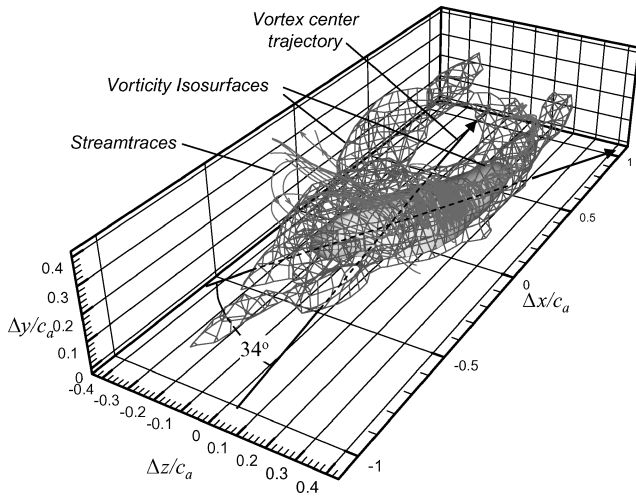

Fig. 6   Pitchwise time-delay correlation coefficient functions for anchor location 2 (see Fig. 2b). Contours in steps of 0.1: black, positive levels and gray, zero. Line AA represents the cut through the correlation space taken in the frame of reference of a hypothetical stator.

Fig. 7   Three-dimensional flowfield associated with streamwise u velocity fluctuations at location 2 determined using linear stochastic estimation and Taylor's hypothesis.

Fig. 8   Spanwise space–time correlation coefficient of upwash velocity component u seen in the frame of reference of a hypothetical stator for anchor location 2 (see Fig. 2b). Contours in steps of 0.1: black, positive levels; gray, zero; and - - - -, negative levels.

to plot the linear stochastic estimate of the instantaneous velocity field associated with velocity fluctuations at location 2. It is easily shown[10] that the best linear estimate is just the product of that velocity fluctuation and the correlation function, for example, for a streamwise velocity fluctuation at 2, u_2, the best linear estimate of the instantaneous flowfield (u_e, v_e, w_e) is

$$u_e(y, Z, \tau) = u_2 R_{uu}(0.07c_a, \Delta y, -4.32c_a, \Delta Z, \tau)$$

$$v_e(y, Z, \tau) = u_2 R_{uv}(0.07c_a, \Delta y, -4.32c_a, \Delta Z, \tau)$$

$$w_e(y, Z, \tau) = u_2 R_{uw}(0.07c_a, \Delta y, -4.32c_a, \Delta Z, \tau) \tag{4}$$

where $\Delta y = y - 0.07c_a$ and $\Delta Z = Z + 4.32c_a$. Figure 7 shows one such instantaneous field estimated for a u_2 fluctuation of unit magnitude. To make the plot easier to interpret, the field has been plotted in terms of flow-aligned coordinates measured from location 2 $(\Delta x, \Delta y, \Delta z)$, the transformation from the variables $(\Delta y, \Delta Z, \tau)$ being made using Taylor's hypothesis, that is, $\Delta x = -\tau U_e$. Streamtraces and vorticity magnitude isosurfaces implied by the estimated field are shown. These clearly show an intense elongated vortical structure skewed at an angle of about 30 deg to the vortex axis. The outer vorticity isosurface even suggests that this structure has a double spiral form, wrapped around the vortex axis. This picture is strongly reminiscent of the helical structures seen by Ragab[6] in direct numerical simulations of a line vortex with unstably large streamwise velocity defect, suggesting a similar mechanism is behind the generation of turbulence in this vortex.

Implications for Engine-Noise Prediction

Although these results illustrate the complexity of the endwall flow and the extreme anisotropy of its turbulence structure, they do not directly reveal the correlated velocity field seen by a set of stator blades. In a real aircraft engine, the rotor tip vortex wakes and the stator blades are in different frames of reference, the former tracing across the latter at the fan tip speed. In the present experiment, which models the flow seen in a rotor-fixed frame, the stators would appear to be translating in the negative Z direction at a speed W_s given by the approach freestream velocity (25.8 m/s) multiplied by the sine of the cascade inlet angle (65.1 deg). Although it is not possible to estimate completely the space–time correlation of velocity fluctuations seen by such a stator blade from the present measurements, we can at least illustrate some of the effects of the frame of reference change upon the correlation function using the grid of two-point measurements made in the tip leakage vortex.

As shown in the Appendix, the space–time correlation function seen in the stator frame of reference is simply related to the
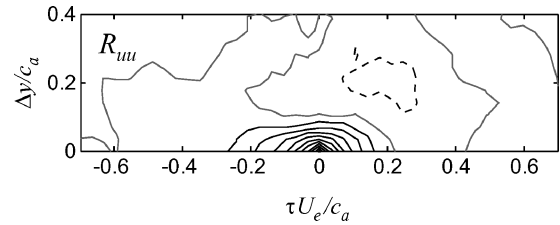
pitchwise-averaged space–time correlation seen in the rotor frame of reference. For example, the two-dimensional spanwise (Δy) time-delay (τ) correlation by a point on the leading edge of a stator moving with apparent speed W_s in the negative Z direction is given by a diagonal slice of slope W_s through the Z-averaged three-dimensional $(\Delta y, \Delta Z, \tau)$ correlation space seen in the rotor fixed frame.

Line AA shown in Fig. 6a illustrates this process showing the path of this diagonal slice through the present (not pitchwise-averaged) correlation data measured in the tip leakage vortex. The corresponding spanwise space–time correlation function (again not pitchwise averaged) seen by the stator is shown in Fig. 8. In both of these figures, we plot the u component because, as it turns out, this is almost exactly the upwash component that would be seen by the stator—the upwash is the most important component from the point of view of broadband noise generation.

Interestingly, the spanwise space–time correlation seen in the tip leakage vortex in the stator frame of reference is quite similar to that seen in the rotor frame (Fig. 4b), that is, that seen on a slice parallel to the time axis. This lack of change is fortuitous, however, because the two cuts happen to lie at roughly equal and opposite angles to the major axis of the highly anisotropic correlation function of the tip leakage vortex turbulence (Fig. 6). In fact, it appears that the correlation function seen by the stator should be strongly dependent upon the exact cut it takes through the rotor correlation space of the tip leakage vortex. In other words, if the turbulence in real engine tip leakage vortices is as anisotropic as that seen here, the velocity correlations seen by a stator in a real engine is likely to be a strong function of the engine geometry and operating point. This suggests the task of accurately predicting the broadband noise generated by such rotor/stator interactions might be a difficult one.

Conclusions

Velocity spectra and space–time correlations have been measured in the wake of a low-speed linear compressor cascade with tip gap. This is a flow in which the tip leakage vortex dominates the turbulence structure in the endwall flow region. It generates a relatively weak tangential velocity field but a strong axial velocity deficit. This deficit appears to be the primary source of turbulence in the vortex and, indeed, the endwall region.

Velocity spectra measured in the leakage vortex are remarkable for their lack of features. Spectral levels here are higher than elsewhere because of the higher turbulence levels, but there are no distinct spectral peaks that might indicate a periodically organized structure. The spectra also do not show the extreme concentration of energy at very low frequencies as would be expected if the vortex were wandering significantly. Indeed, two-point correlation measurements show conclusively that low-frequency wandering is not present.

The two-point measurements also show no correlation between turbulent motions in the wakes or leakage vortices shed by adjacent blades. They do, however, show the presence of significant large-scale structure within the leakage vortex flow itself. This structure appears highly anisotropic both in terms of the dissimilarity between the correlations of different velocity components and in terms of the scales of the various correlation functions, which in most cases are a strong function of direction. In particular, pitchwise space–time correlations measured just beneath the vortex center show an elongated

elliptical region of strong correlation that extends diagonally across the vortex. Linear stochastic estimation of the instantaneous velocity field associated with velocity fluctuations beneath the vortex appears to show that these correlations are produced by spirallike coherent structures that make an angle of about 30 deg to the vortex axis. These structures are reminiscent of helical structures seen by Ragab[6] in direct numerical simulations of a line vortex with unstably large streamwise velocity defect, suggesting a similar mechanism might be behind the generation of turbulence in this vortex. Examination of the correlation data in the leakage vortex from the point of view of a hypothetical stator blade suggests that, because of the anisotropy in turbulence structure, velocity correlations seen by a stator in a real engine are likely to be a strong function of engine geometry and operating point.

Appendix: Relationship Between the Space–Time Correlation in Stator and Rotor Frames

Consider the wake of a linear cascade of rotor blades impinging on a row of stators as seen from the rotor frame of reference. The upwash velocity field at the stator leading-edge plane in the rotor frame of reference is denoted by

$$q = q(X, y, Z, t) \tag{A1}$$

where X, y, and Z are the rotor-fixed axial, spanwise, and pitchwise coordinates (Fig. 1). The upwash velocity field at the stator leading-edge plane in the stator frame of reference is denoted by

$$q_s = q_s(X_s, y_s, Z_s, t) \tag{A2}$$

where subscript s denotes a stator-fixed coordinate. The radial coordinates y and y_s and the axial coordinates X and X_s are measured from the same position, and the tangential coordinates Z and Z_s are coincident at $t = 0$. The apparent stator pitchwise velocity W_s is directed opposite to Z. Thus, we have the relation

$$q_s(X_s, y_s, Z_s, t) = q(X, y, Z - W_s t, t) \tag{A3}$$

The time-delay correlation between two points in the stator frame of reference (X_s, y_s, Z_s) and $(X_s + \Delta X_s, y_s + \Delta y_s, Z_s + \Delta Z_s)$ is defined as

$$\operatorname*{Lim}_{T \to \infty} \frac{1}{2T} \int_{-T}^{T} q_s(X_s, y_s Z_s, t) q_s(X_s + \Delta X_s, y_s$$

$$+ \Delta y_s, Z_s + \Delta Z_s, t + \tau) \, dt \tag{A4}$$

Rewriting q_s in terms of q gives

$$\operatorname*{Lim}_{T \to \infty} \frac{1}{2T} \int_{-T}^{T} q(X, y, Z - W_s t, t) q(X + \Delta X, y$$

$$+ \Delta y, Z + \Delta Z - W_s(t + \tau), t + \tau) \, dt \tag{A5}$$

The result of this integral is independent of Z and t because the flow is ergodic and (on time average) periodic in Z. Therefore, the preceding integral can be averaged with respect to Z without changing its value, that is,

$$\operatorname*{Lim}_{R_z \to \infty} \frac{1}{2R_z} \int_{-R_s}^{R_s} \operatorname*{Lim}_{T \to \infty} \frac{1}{2T} \int_{-T}^{T} q(X, y, Z - W_s t, t)$$

$$\times q(X + \Delta X, y + \Delta y, Z + \Delta Z$$

$$- W_s(t + \tau), t + \tau) \, dt \, dZ \tag{A6}$$

where R_z denotes the region of Z integration. Reversing the order of integration gives

$$\operatorname*{Lim}_{T \to \infty} \frac{1}{2T} \int_{-T}^{T} \operatorname*{Lim}_{R_z \to \infty} \frac{1}{2R_z} \int_{-R_z}^{R_z} q(X, y, Z - W_s t, t)$$

$$\times q(X + \Delta X, y + \Delta y, Z + \Delta Z - W_s(t + \tau), t + \tau) \, dZ \, dt \tag{A7}$$

Because the inner integration is carried out over all Z, it makes no difference whether $Z - W_s t$ or Z alone appears in the argument of q. So, the correlation becomes

$$\operatorname*{Lim}_{T \to \infty} \frac{1}{2T} \int_{-T}^{T} \operatorname*{Lim}_{R_z \to \infty} \frac{1}{2R_z} \int_{-R_z}^{R_z} q(X, y, Z, t)$$

$$\times q(X + \Delta X, y + \Delta y, Z + \Delta Z - W_s \tau, t + \tau) \, dZ \, dt \tag{A8}$$

Again, reversing the order of integration gives

$$\operatorname*{Lim}_{R_z \to \infty} \frac{1}{2R_z} \int_{-R_s}^{R_s} \operatorname*{Lim}_{T \to \infty} \frac{1}{2T} \int_{-T}^{T} q(X, y, Z, t)$$

$$\times q(X + \Delta X, y + \Delta y, Z + \Delta Z - W_s \tau, t + \tau) \, dt \, dZ \tag{A9}$$

This result is nothing more than the pitchwise average of the two-point space–time correlation in the rotor-fixed frame, with ΔZ replaced by $\Delta Z - W_s \tau$. We can thus infer the velocity correlation function seen in the stator frame from that seen in the rotor frame.

References

[1]Muthanna, C., and Devenport, W. J., "Wake of a Compressor Cascade with Tip Gap, Part 1: Mean Flow and Turbulence Structure," *AIAA Journal*, Vol. 42, No. 11, 2004, pp. 2320–2331.

[2]Wang, Y., and Devenport, W. J., "Wake of a Compressor Cascade with Tip Gap, Part 2: Effects of Endwall Motion," *AIAA Journal*, Vol. 42, No. 11, 2004, pp. 2332–2340.

[3]Hanson, D. B., "Quantification of Inflow Turbulence for Prediction of Cascade Broadband Noise," International Inst. of Acoustics and Vibration, 5th International Congress on Sound and Vibration, Paper 990544, Auburn, AL, Dec. 1997.

[4]Ganz, U., Glegg, S. A. L., and Joppa, A., "Measurement and Prediction of Broadband Fan Noise," AIAA Paper 98-2316, 1998.

[5]Mayer, E. W., and Powell, K. G., "Similarity Solutions for Viscous Vortex Cores," *Journal of Fluid Mechanics*, Vol. 238, 1992, pp. 487–507.

[6]Ragab, S. A., "Direct Numerical Simulation of Instability Waves in a Trailing Vortex," AIAA Paper 95-0591, Jan. 1995.

[7]Antonia, R. A., and Britz, D., "Phase-Averaging in the Turbulent Far Wake," *Experiments in Fluids*, Vol. 7, No. 2, 1989, pp. 138–142.

[8]Devenport, W. J., Rife, M. C., Liapis, S. I., and Follin, G. J., "The Structure and Development of a Wing-Tip Vortex," *Journal of Fluid Mechanics*, Vol. 312, 1996, pp. 67–106.

[9]Kline, S. J., and McClintock, F. A., "Describing Uncertainties in Single Sample Experiments," *Mechanical Engineering*, Vol. 75, No. 1, 1953, p. 3.

[10]Adrian, R. J., "Stochastic Estimation of the Structure of Turbulent Fields," *Eddy Structure Identification*, CISM Courses and Lectures No. 353, edited by J. P. Bonnet, Springer, New York, 1996, pp. 146–195.

R. So
Associate Editor